Soft Matter

Accepted Manuscript

ROYAL SOCIETY OF CHEMISTRY

www.rsc.org/softmatter

ARTICLE TYPE www. rsc.org/xxxxxx | XXXXXXXX

Self-assembly of three-dimensional open structures using patchy colloidal particles

D. Zeb Rocklin,[a]* and Xiaoming Mao,[a]

Open structures can display a number of unusual properties, including a negative Poisson's ratio, negative thermal expansion, and holographic elasticity, and have many interesting applications in engineering. However, it is a grand challenge to self-assemble open structures at the colloidal scale, where short-range interactions and low coordination number can leave them mechanically unstable. In this paper we discuss the self-assembly of three-dimensional open structures using triblock Janus particles, which have two large attractive patches that can form multiple bonds, separated by a band with purely hard-sphere repulsion. Such surface patterning leads to open structures that are stabilized by orientational entropy (in an order-by-disorder effect) and selected over close-packed structures by vibrational entropy. For different patch sizes the particles can form into either tetrahedral or octahedral structural motifs which then compose open lattices, including the pyrochlore, the hexagonal tetrastack and the perovskite lattices. Using an analytic theory, we examine the phase diagrams of these possible open and close-packed structures for triblock Janus particles and characterize the mechanical properties of these structures. Our theory leads to rational designs of particles for the self-assembly of three-dimensional colloidal structures that are possible using current experimental techniques.

1 Introduction

Open structures are those in which the microscopic constituents occupy only a low fraction of the total volume, leaving open space between them and allowing the structures to undergo a richer variety of fluctuations and deformations than close-packed structures. They possess striking properties such as negative Poisson's ratio [1–3], negative thermal expansion [4,5], holographic elasticity [2,6] and beyond [7–10], leading to many interesting applications in engineering.

A structure can be open at different scales, depending on the size of the constituents and the open space. Zeolite, a natural aluminosilicate mineral, is an example of an open lattice structure with pores (open spaces) at the scale of Angstroms [7,11]. Nature also offers us structures that are open at larger length scales, such as foams and bones, but these structures are generally disordered.

Obtaining open structures with pores at the colloidal scale is not only desirable for such applications as photonic crystals [12–15], but also presents a fundamentally interesting question in physics. The challenge comes from the proximity of these open structures to *mechanical instability*. The existence of zero-energy deformations of the open structure raises the possibility of its collapse into a close-packed structure. The stability of a colloidal structure can be explained by the counting argument due to Maxwell [16]: that for a structure to be mechanically stable, its total number of constraints must equal or exceed its total number of internal degrees of freedom. This argument, applied to simple colloidal particles with only isotropic central force interactions between nearest neighbor particles, leads to the stability criterion $z > z_c = 2d$ where z is the coordination number and d is the spatial dimension, and the special state with $z = z_c$ is called the *isostatic point*. According to this criterion, most open lattices are not stable. For example, the diamond lattice has $z = 4 < 2d$ and is below isostaticity and the pyrochlore lattice has $z = 6 = 2d$ and is at the verge of instability. Another interesting example is a lattice of corner-sharing octahedral cells, which has $z = 8 > 2d$ but still has some floppy modes due to redundancy of constraints. We refer to this perovskite-like lattice as perovskite, although it has open space between octahedral cells where additional atoms would sit in mineral perovskite. Fig. 1 shows examples of these lattices and their floppy modes.

Thus, to obtain open lattice structures at the colloidal scale additional interactions beyond a simple nearest neighbor isotropic potential have to be added to provide mechanical stability, preventing the structure from collapsing. Various designs have been proposed [17–23], which require complicated inter-particle potentials that are difficult to realize in experiment.

Remarkably, an open two-dimensional kagome lattice has been self-assembled using triblock Janus colloidal particles very recently [24]. Janus colloidal particles have chemical coatings that cover a fraction of their surfaces ("patches"), making their interaction potential anisotropic. The triblock Janus particles used in the experiment in Ref. [24] are characterized by patches at their north and south poles of short range hydrophobic attraction of depth $\sim 10k_BT$ and a middle band of

[a] *Department of Physics, University of Michigan, 450 Church Street, Ann Arbor, MI 48109, USA*
* *drocklin@umich.edu*

strongly screened electrostatic repulsion[25,26]. The short range nature of the inter-particle potential in this triblock Janus particle system does not directly provide more energetic constraints for stability. Instead, it has been found that entropy plays the important role of stabilizing open lattices formed by these triblock Janus particles because, among all structures of degenerate potential energy, the open lattice permits the most rotational and vibrational fluctuations of the constituent particles[27,28].

In this work, we explore the self-assembly of three-dimensional lattices using the triblock Janus particle based on this entropic stabilization/selection mechanism. We develop the formalism first used in Refs.[27,28] to incorporate three-dimensional rotations of Janus particles which stabilize open lattices in three dimensions. We show that depending on the size of the attractive patches, these particles can either form a perovskite lattice or a mixed phase of pyrochlore/hexagonal tetrastack (HT) lattices (Fig. 1) and that under pressure they can collapse into a close-packed face centered cubic (FCC) lattice. A kagome bilayer, which includes octahedral cells, has already been observed[24]— many such layers would produce a perovskite lattice. The self-assembly of the pyrochlore/HT lattices has been examined in Ref.[22] using simulations, with which we compare our results to in Sec. 3.3. In this work we analytically describe the role of entropy in selecting the phases and characterize the phase diagram of this system using a harmonic approximation of the entropic effects and lattice dynamics calculations. Our theory opens the door to greatly simplified designs of building blocks for the self-assembly of three-dimensional open lattices.

2 Model

2.1 Statistics of patchy particles

Generally, we may describe the equilibrium statistical mechanics of a set of anisotropic particles via the partition function[27,28]

$$\mathscr{Z} = \int \exp\left[-\frac{1}{k_B T} H(\{\mathbf{r}_j, \hat{n}_j\})\right] \prod_j d\mathbf{r}_j d\hat{n}_j, \tag{1}$$

where the Hamiltonian H depends on the positions $\mathbf{r}_j$ and $\hat{n}_j$ orientations of the particles and k_B is the Boltzmann constant and T the temperature.

The particles we consider, *triblock Janus particles*, have two attractive patches separated by a repulsive band, as shown in Fig. 2. These particles have a hardcore repulsion when their separation is close to their diameter, a. Additionally, there is a short-range attraction between particles whose patches are oriented towards one another, permitting the formation of bonds.

We now consider a lattice of such particles, which may in general include both *attractive bonds*, where particles contact each other in their attractive patches, and *repulsive bonds*, where the particles are held close to each other by the lattice structure, so that thermal fluctuations and hardcore repulsions keep them apart and impose a free energy cost. The strength of the attractive bonds can be around $\sim 10 k_B T$[25,26], so thermal fluctuations will not give configurations with broken bonds appreciable Boltzmann weight. We may then restrict our ensemble to a particular bond structure and integrate out the particle orientations $\hat{n}_j$ from the partition function of Eq. (1), and the result will be a degeneracy factor $\Omega_j(\{\mathbf{r}_i\})$ proportionate to the number of orientations (all of which share the same potential energy) which keep all the attractive bonds within attractive patches. The orientational entropy of a particle depends on the relative positions of each particle with which it has an attractive bond, and is related to the degeneracy factor via[27,28]

$$s_j = k_B \ln \Omega_j(\{\mathbf{r}_i\}). \tag{2}$$

This term accounts entirely for the effect of particle orientations given in Eq. (1), leading to an effective Hamiltonian which depends only on particle *positions*.

For the case of a triblock Janus particle j with unit vectors $\hat{e}_{ij}$ to each of its attractively-bonded neighbors i. These bonds lie within an attractive patch provided that

$$\left|\hat{e}_{ij} \cdot \hat{n}_j\right| \geq \cos\phi_0, \tag{3}$$

where ϕ_0 is the patch size, the maximum angle between a point in the patch and the particle's "north pole", the center of an attractive patch. Positive (negative) values of $\hat{e}_{ij} \cdot \hat{n}_j$ correspond to bonds that lie in the particle's northern (southern) hemisphere. Thus, the degeneracy factor is simply

$$\Omega_j(\{\mathbf{r}_i\}) = \int d\hat{n}_j \prod_i \Theta\left[\left|\hat{e}_{ij} \cdot \hat{n}_j\right| - \cos\phi_0\right], \tag{4}$$

where $\Theta(\cdot)$ is the Heaviside step function.

This entropy is maximized when all bonds lie as close as possible to either the north or south pole of a particle as is permitted by the hardcore repulsion between particles. Three-dimensional open lattices can then be formed from rigid octahedral or tetrahedral cells (depending on whether the patches are large enough to support four bonds or only three) that meet at their corners (centers of triblock Janus particles) and directly oppose one another there. This permits the formation of three types of three-dimensional lattices: the pyrochlore, the hexagonal tetrastack (HT) and the perovskite, cf. Fig. 1.

In the pyrochlore and HT lattices, a particle forms a rigid tetrahedral structure with its three northern neighbors, and another with its three southern neighbors. In the perovskite, any particle lies at a vertex joining two octahedra and has four bonds in each of its attractive patches. Such structures are possible when the patch size is large enough to support these three or four neighboring particles, so that above $\phi_0^{\min(4)} = 45^\circ$

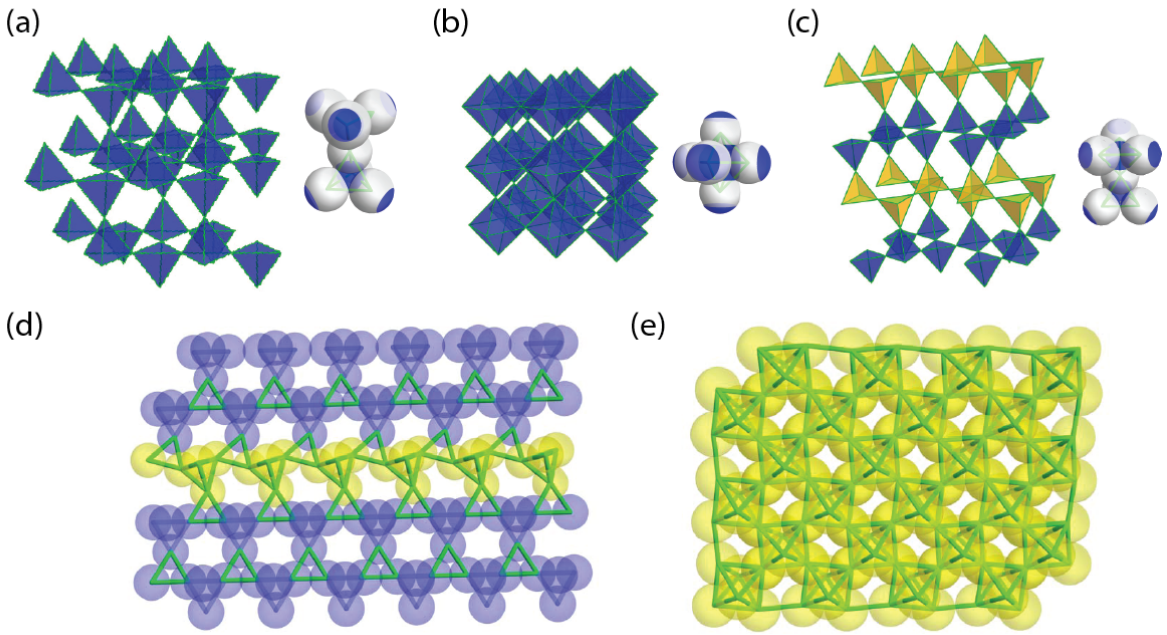

Fig. 1 Open lattices (a-c), where structures of the lattices are shown on the left and the triblock Janus particles forming the basic motifs are shown on the right) and the floppy modes (d, e) such structures have if composed of isotropic particles rather than triblock Janus particles. (a) Pyrochlore lattice, with tetrahedral cells and six bonds for each triblock Janus particle. (b) Perovskite-like lattice, with octahedral cells and eight bonds per particle. (c) Hexagonal tetrastack (HT) lattice. Otherwise identical to the perovskite structure, blue and yellow layers are rotated $\alpha = 60^\circ$ relative to one another, so that the bonds of the triblock Janus particles that lie at the juncture between layers have a permanent twist. (d) Floppy modes in a layer of the pyrochlore lattice, with green lines indicating bonds between spherical particles. A single floppy mode is present in the layer: each of the yellow tetrahedral cells has been rotated about the axis perpendicular to the plane of the layer without changing the relative positions of the blue particles or particles in other other layers. To leading order, such modes don't alter any bond lengths and so cost zero energy in systems with only isotropic central forces. (e) A floppy mode in the perovskite-like lattice, with every particle in the layer affected. Zero energy modes of the perovskite-like lattice rotate all of the octahedral cells in a layer relative to their neighbors, while leaving other layers unaltered. These floppy modes, as shown in (d,e), can lead to the collapse of open lattices if the composing particles are isotropic with short-range interactions.

four bonds per patch become possible (and energetically favored), leading to octahedral cells. Between this patch size and $\phi_0^{\min(3)} = \arccos(\sqrt{2/3}) \approx 35.3^\circ$ only three bonds are possible, leading to tetrahedral cells.

Any distortions of these rigid polyhedra will carry finite energy costs but, as discussed in the introduction, floppy modes exist in these lattices in which only the *angles* between neighboring polyhedra change (Fig. 1). Floppy modes in these lattices have been named Rigid Unit Modes (RUMs)[5] in the research of open structure crystals. Such RUMs are the dominant thermal fluctuation present in a lattice of triblock Janus particles, with the bond length fluctuations much smaller than bond angle fluctuations[27].

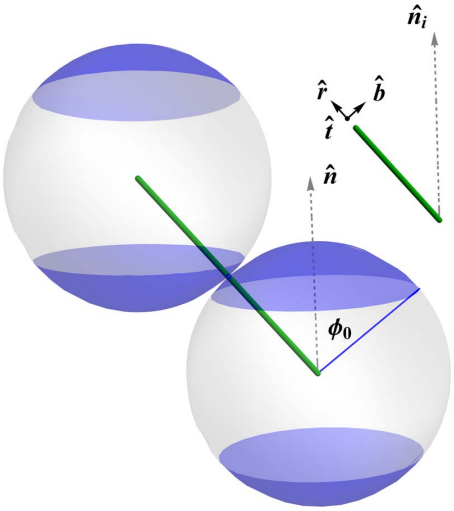

Fig. 2 Triblock Janus particles have two circular attractive patches separated by a repulsive band. The orientation of a triblock Janus particle i is given by its "north pole", $\hat{n}_i$. The patch size, ϕ_0, is the angle between the edge of a patch and its center. Two adjacent particles are bonded attractively if the contact point lies within contact patches on both particles. The north pole $\hat{n}_i$ can assume any orientation that keeps all of the northern bonds in the attractive patch, but has an average or *preferred* orientation equal to the average direction of all of the northern bonds. The movement of a particle relative to particle i can be decomposed into movements along the radial direction, $\hat{r}$, the bending direction $\hat{b}$ which is orthogonal to $\hat{r}$ but points toward the preferred orientation of particle i, and the twisting direction $\hat{t}$ which is orthogonal to both $\hat{r}$ and the preferred $\hat{n}_i$.

2.2 Analytic model of bending rigidity

In order to analyze the dynamics of the three-dimensional lattice, we approximate the effects of a particle's orientational entropy through an analytic effective energy incorporating only the rigid body rotations of a particle's northern bonds about its southern ones:

$$U_r = \frac{1}{2}\kappa_t \alpha^2 + \frac{1}{2}\kappa_b \beta^2, \tag{5}$$

where κ_t is the twisting modulus and κ_b the bending modulus. The *bending angle* β, which can be decomposed into two components, β_x and β_y, is the angle by which the northern cell differs from perfectly opposing the southern cell, as depicted in Fig. 3. The *twisting angle* α is the angle by which the northern cell is rotated about its own axis, with $\alpha = 0$ corresponding to northern bonds that are (for $\beta = 0$) collinear with southern ones. For a given set of particle positions, a particle's bending and twisting angles are determined by decomposing the relative movements of each of its neighbors along their bending direction $\hat{b}$ and twisting direction $\hat{t}$ respectively, as depicted in Fig. 2.

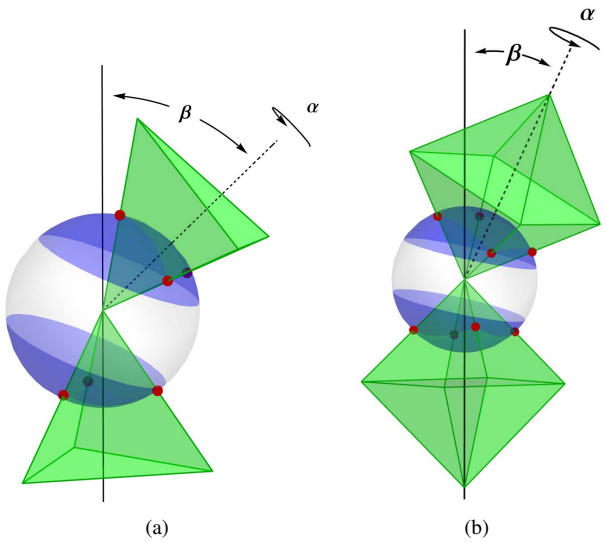

Fig. 3 The tetrahedral (a) or octahedral (b) cells that a triblock Janus particle composes with its neighbors, which it contacts at points marked by red dots. Lattice fluctuations may twist the northern cell through an angle α about its axis and bend it through an angle β relative to the southern cell. As the bending angle increases, fewer orientations of the central triblock Janus particle are possible, lowering the weight of such configurations in the lattice and creating an effective modulus against bending.

A free triblock Janus particle—that is, one whose bonds are free to undergo any rigid rotation—has simple Gaussian fluctuations in the harmonic approximation of Eq. (5), leading to a mean square bending angle

$$\langle \beta^2 \rangle = 2\frac{k_B T}{\kappa_b}. \tag{6}$$

Separately, the mean square bending angle of a free triblock

Janus particle may be determined numerically from the degeneracy factor of Eq. (4), expressed now in terms of the bending and twisting angles rather than the more general neighbor positions:

$$\langle \beta^2 \rangle = \frac{\int d^2\beta \, d\alpha \, \Omega_j(\beta,\alpha)\beta^2}{\int d^2\beta \, d\alpha \, \Omega_j(\beta,\alpha)}. \tag{7}$$

Equating the two expressions allows us to select a bending modulus that reproduces the magnitude of bending angle fluctuations. Treating the true degeneracy factor, plotted in Fig. 4, as a Gaussian amounts to neglecting higher-order terms in the bending and twisting angles. For patch sizes very close to the minimum sizes necessary to support all of the bonds, the bending modulus diverges as $\left(\phi_0 - \phi_0^{\min}\right)^{-2}$, as depicted in Fig. 5. Within our analytic model, it is this bending modulus that imposes an effective cost on otherwise zero-energy modes and ensures that bending and twisting angles remain small.

For a *free* triblock Janus particle, the twisting modulus κ_t proves to be zero. This is because for a given Janus particle orientation, there is a one-to-one correspondence between those bending angles allowed by a finite twisting angle α and those allowed at $\alpha = 0$, so that twisting the cells does not affect the overall degeneracy. If, instead, the bending angle were held fixed at $\beta = 0$, twisting to $\alpha = 30^\circ$ would decrease Ω by about $1/3$ of its maximum value[27], corresponding to a twisting modulus below $1 k_B T$.

In a lattice, bending or twisting the bonds of a given triblock Janus particle can only be accomplished by bending and twisting other bonds in the lattice. Thus, certain values of α are not accessible in a lattice because they necessarily involve bending angles that break bonds (e.g., for a patch size that requires $\beta \leq 1^\circ$, $\alpha = 20^\circ$ is not accessible). Thus, in a lattice the twisting angles will be restricted to small deviations from their optimum value (which is $\alpha = 0^\circ$ except for in particles at junctions between layers in the HT lattice, for which it is $\alpha = 60^\circ$). As we will see below, the bending modulus gives all the zero modes of the lattice an effective energy, and the inclusion of a finite twisting modulus (which would be orders of magnitude smaller) in our model would have only a very small effect. The dependence of Ω_j on the bending angle in each of these scenarios is shown in Fig. 4.

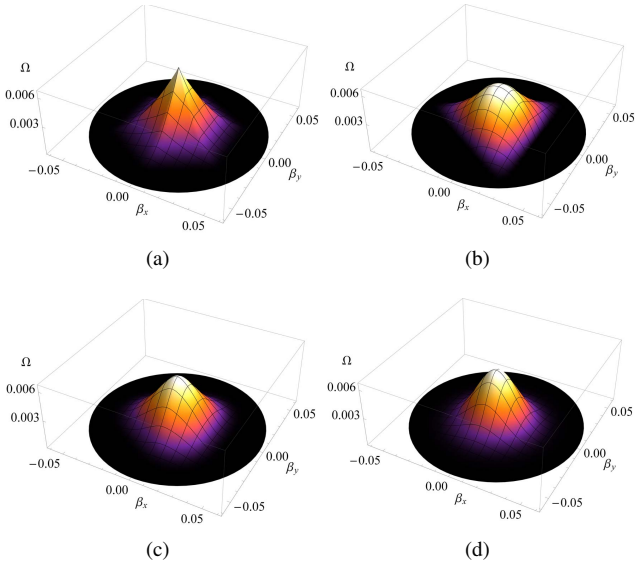

Fig. 4 The weight Ω, or total fraction of triblock Janus particle orientations associated with bending angle components (β_x, β_y) of a triblock Janus particle with patch size $\phi_0 = 36.1^\circ$ barely large enough to support its three bonds per patch. In (a), twisting angle α is fixed at 0°, as in the pyrochlore lattice, and there is hexagonal symmetry associated with the six bond directions. In (b), $\alpha = 60^\circ$, as in the HT structure, leading to triangular symmetry as some bonds oppose one another. In (c), all values of α are averaged over, as for isolated tetrahedral cells not held in place by the lattice. In (d), the harmonic approximation to the weight Ω used in the analytic model shares the width of the true Ω, but not its rotational asymmetry.

2.3 Lattice energetics

Having accounted for the effects of orientational entropy, we may now construct an effective Hamiltonian for a lattice purely in terms of the *positions* of the triblock Janus particles. In the lattice, we may take these positions as

$$\mathbf{r}_j = \mathbf{R}_j + \mathbf{u}_j, \tag{8}$$

where $\mathbf{R}_j$ is the lattice site and the displacement $\mathbf{u}_j$ is small compared to the particle spacing. This then allows us to formulate the central force interaction between bonded particles as a harmonic spring, so that

$$V_{\rm cf}(\mathbf{u}_i - \mathbf{u}_j) = \frac{k_{a(r)}}{2} \frac{\left[(\mathbf{R}_i - \mathbf{R}_j)\cdot(\mathbf{u}_i - \mathbf{u}_j)\right]^2}{(\mathbf{R}_i - \mathbf{R}_j)^2}, \tag{9}$$

where the effective spring constant is $k_{a(r)}$ for attractive (repulsive) bonds. Thus, the effective Hamiltonian, incorporating both the central-force and rotational-entropy terms, is

$$H_{\rm eff} = \sum_{\langle i,j \rangle} V_{\rm cf}(\mathbf{u}_i - \mathbf{u}_j) + \sum_i \frac{\kappa_b}{2} \beta_i^2, \tag{10}$$

where the first sum is over bonded neighbors, with $k_{i,j}$ differing depending on whether the bond is attractive or repulsive.

General lattice displacements will distort as well as rotate the tetrahedral cells depicted in Fig. 2. However, the angle by which the bending components of the displacements— combined vectorially— rotates the tetrahedron from its $\mathbf{u} = 0$ position remains well-defined. The bending angle β_i is the change

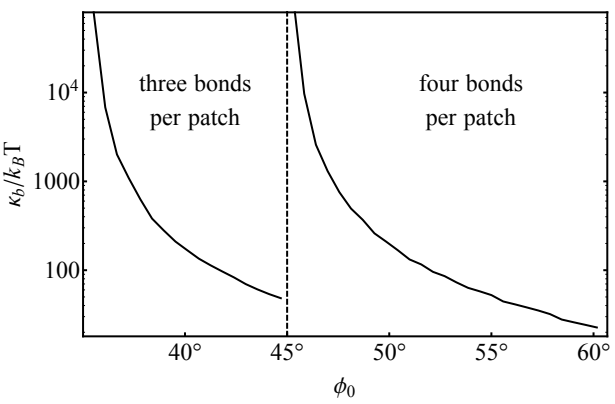

Fig. 5 The effective bending modulus κ_b, in units of temperature, as a function of ϕ_0, the angular half-width of the attractive patch. Between $\phi_0 \approx 35.3^\circ$ and $\phi_0 = 45^\circ$ the patch is able to support a maximum of three bonds, as in the pyrochlore lattice. Above 45°, the patch supports four bonds, as in the perovskite lattice.

in the angle between the surface normal vectors of the two tetrahedra (or octahedra) in which particle i lies. Note that this depends on the positions of all of particle i's neighbors, leading to an effective next-nearest neighbor coupling.

From this harmonic Hamiltonian, the dynamical matrix associated with a crystal lattice may be generated using standard techniques[29]. The phonon dispersions for the dynamical matrices associated with the pyrochlore and perovskite lattices are shown in Fig. 6.

In a pyrochlore lattice with L^3 tetrahedral cells the high-symmetry planes have the structure of the kagome lattice. As discussed in Refs.[27,28,31], each such kagome lattice has $O(L)$ zero modes consisting of twists applied to lines of triangular cells. The analogous mode of the pyrochlore lattice, a line of twisting tetrahedral cells, is depicted in Figure 1. The pyrochlore lattice has $O(L^2)$ such zero-energy (for $\kappa_b = 0$) modes. It is these modes which render the $\kappa_b = 0$ pyrochlore lattice unstable, and which are most strongly modified by the inclusion of a finite bending modulus. The HT lattice similarly has $O(L^2)$ zero modes, with $1/3$ of the kagome modes replaced by displacements of columns of tetrahedra in the direction perpendicular to the blue and yellow planes in Figure 1.

In the perovskite lattice, which is above the isostatic point, the only zero modes are a number $O(L)$ in which an entire *plane* of octahedra rotate in concert, as depicted in Figure 1. Similar to the pyrochlore lattice, these are the modes most strongly modified by the bending modulus. The presence of the zero modes and the effect of the bending modulus on them are evident in the dispersions in Figure 6.

For the self-assembly examined in Ref.[27], the bending modulus is large in the sense that $\kappa_b \approx 33 k_B T$ permits only small

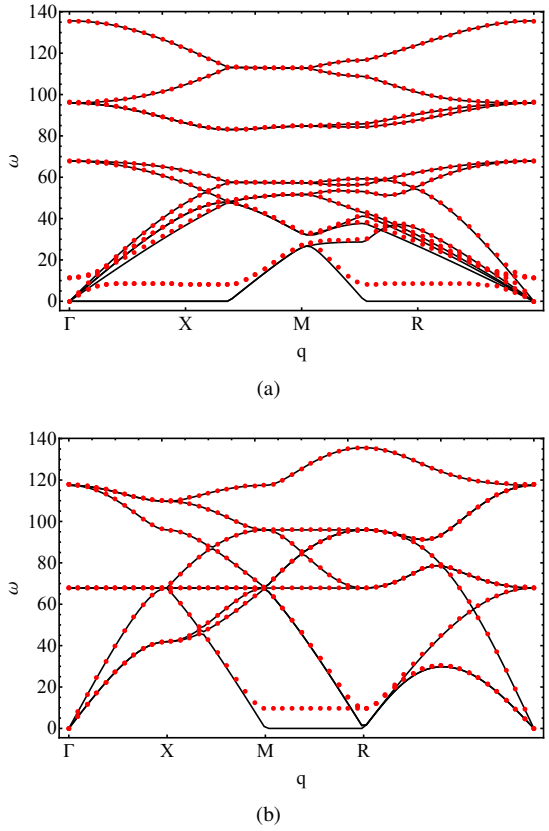

Fig. 6 Phonon dispersions for the pyrochlore (a) and perovskite (b) lattices as the reciprocal vector q passes between points in the Brillouin zone[30]. The black solid curves show the case of $k_a a^2 = 2300 k_B T$ and $\kappa_b = 0$, which includes a plane of zero modes in the pyrochlore lattice and a line of zero modes in the perovskite lattice, agreeing with the counting of floppy modes discussed above. These modes are lifted by the inclusion of $\kappa_b = 33 k_B T$ (red dotted curves). The values of k_a and κ_b are taken from Ref.[27].

bending angles, but small compared to the central forces modulus, $k_a a^2 \approx 2300 k_B T$. As such, the effect of orientational entropy amounts only to a linear perturbation in the frequencies of most of the modes of the lattice. However, for the zero modes, there is a $O(\sqrt{\kappa_b})$ increase in frequency, as seen in Figure 6. The effective bending modulus has a similar effect on the zero modes of the perovskite lattice.

In the absence of this orientational entropy effect, the zero modes of the lattices would permit large distortions of the lattices, destroying mechanical stability. The patchiness of the particles prevents arbitrary rotations of the tetrahedral units, and the orientational entropy of the triblock Janus particles favors the $\beta = 0$ configuration over distortions to the lattices.

At finite temperature and fixed volume, the phase of the particles is determined by their free energy. As discussed in Ref.[28], the free energy per particle (not including a constant

bonding energy) may be expressed in terms of the momentum-space dynamical matrix $\mathscr{D}(\vec{q})$, which describes the energy of small periodic deformations of the lattice, as

$$f(\kappa_b) = \frac{k_B T}{2n_c} v_0 \int_{1BZ} \frac{d^d\vec{q}}{(2\pi)^d} \ln\det \mathscr{D}(\vec{q}, \kappa_b), \qquad (11)$$

where v_0 is the volume of a unit cell, n_c is the number of particles per unit cell, and the integral is over the first Brillouin zone.

3 Results and Discussion

3.1 Dependence of free energy on patch size

We calculated the change of lattice free energy per particle as a function of bending modulus which comes from orientational entropy of the particles and is controlled by the patch size as show in Fig. 5, and the results are shown in Fig. 7. This reflects the decreased entropy from limiting lattice distortions to ones that keep all bonds within attractive patches. For the pyrochlore lattice, this increase is $O(\sqrt{\kappa_b})$ for small κ_b, reflecting the modifications to its $O(L^2)$ zero modes. The HT lattice, with its similar structure, has nearly identical free energies, suggesting that mixtures of pyrochlore and HT structures may form, as noted earlier by[22].

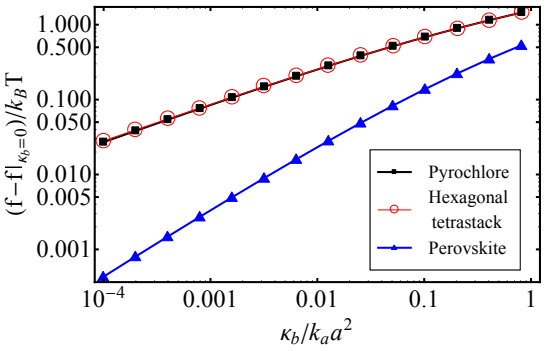

Fig. 7 The free energy per particle of a lattice with bending modulus κ_b relative to a lattice with $\kappa_b = 0$. For the pyrochlore (black curve with square points) and hexagonal tetrastack lattices (red curve with open circular points), there are nearly identical $\sim\sqrt{\kappa_b}$ contributions from surfaces of modes that are zero-energy for $\kappa_b = 0$. For the perovskite lattice (blue curve with triangular points), which has only a line of such modes, the free energy increase is linear for small κ_b.

In contrast to the isostatic pyrochlore and HT lattices, the perovskite lattice with only a number $O(L)$ of such zero modes has a slower increase $O(\kappa_b)$ in the free energy as bending modulus increases.

3.2 Comparison to close-packed structure

Competing with the open structures above are the close-packed face-centered cubic (FCC) lattice, as well as the hexagonal close-packed lattice, which has nearly identical free energies[32]. In such a lattice, each triblock Janus particle has twelve nearest neighbors, even though not all of them lie within the attractive patches, as can be seen in Fig. 8. Such a close-packed structure is favored by a finite pressure, but is disfavored by entropic considerations. These repulsive particle-particle interactions derive from the shorter-range hardcore repulsion rather than the 10 nm hydrophobic attraction[24] and consequently have a greater spring constant $k_r \approx 20k_a$[27] and substantially inhibit the fluctuations in the positions of the triblock Janus particles. This leads to rises in free energy as shown in Fig. 9. Both the bending modulus and the repulsive bonds tend to limit the position fluctuations of the triblock Janus particles in the same way, so that the bending modulus has a greater effect on the open structures than on the FCC lattice, leading to closer free energies as κ_b increases. The free energy differences are greater for the pyrochlore than the perovskite lattices, reflecting the fact that triblock Janus particles with patch size appropriate to the pyrochlore lattice have six repulsive bonds per particle in the FCC lattice, while perovskite-size patches lead to four repulsive bonds in the FCC lattice.

Transforming to a finite-pressure system via a Legendre transformation, one obtains the Gibbs free energy per particle

$$g = f + pv, \qquad (12)$$

where p is the pressure and v the volume per particle. From this, one may determine the dominant phase at a given patch size and pressure, as shown in Figure 10. At low pressures, either the perovskite lattice or a mixture of pyrochlore and HT (depending on whether the patch size is enough to allow four bonds) is present. The perovskite lattice, despite having a lower free energy difference (cf. Fig. 9) is present at higher pressures than the pyrochlore owing to its denser structure.

Note that unlike the dimensionless moduli against bond length fluctuations, $ka^2/2\pi k_B T$, which decrease with increasing temperature, the dimensionless bending modulus has entropic rather than energetic origins and so does not scale with temperature. This leads to nontrivial temperature dependence in the dynamical matrix and corrections to the phase diagram in Fig. 10, but because the bending modulus is much weaker than the central-force moduli at all relevant temperatures, this effect on the free energy is very small.

3.3 Comparison of model to experiment and simulation

In developing our analytic model, we made a number of approximations. In treating the effect of patchiness as purely

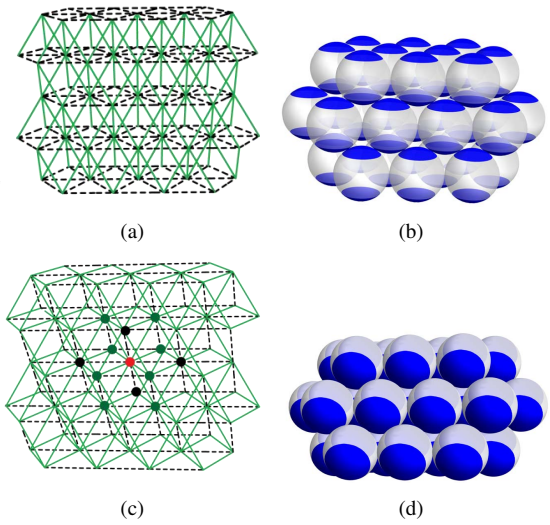

Fig. 8 Close-packed FCC lattices formed by triblock Janus particles. (a) and (b) show the FCC lattice in which each triblock Janus particle has 6 bonds in its attractive patches, corresponding to the patch size that supports the pyrochlore/HT lattices at zero pressure. (c) and (d) show the FCC lattice in which each triblock Janus particle has 8 bonds in its attractive patches, corresponding to the patch size that supports the perovskite lattices at zero pressure. In (a) and (c), attractive bonds are denoted by green lines and repulsive bonds by dashed black lines. The green dots in (c) represent sites attractively bonded to the red site, and the black dots to repulsively bonded sites.

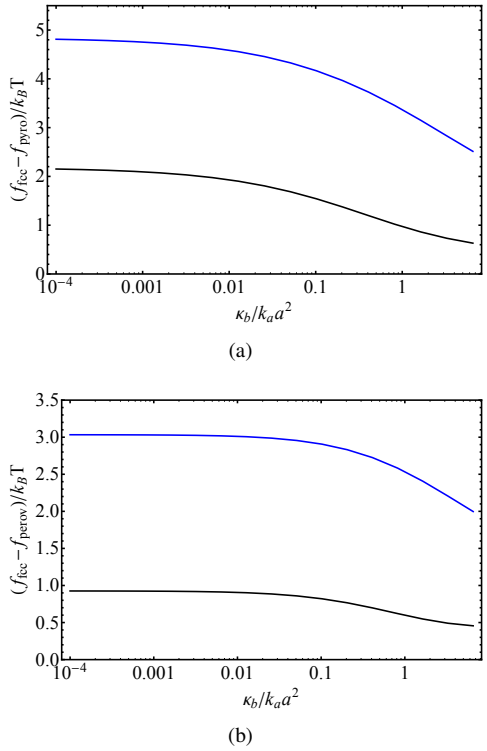

Fig. 9 (a) Free energy difference between the FCC and the pyrochlore lattices as a function of κ_b/k_aa^2 for $k_r = 20$ (top, blue curve) and $k_r = 1$ (bottom, black curve). (b) Free energy difference between the FCC and the perovskite lattices as a function of κ_b/k_aa^2 for $k_r = 20$ (top, blue curve) and $k_r = 1$ (bottom, black curve).

entropic, we assume a system in which the range of interactions is much shorter than the angular fluctuations. This is justified in experimental systems[24], in which the range of the hydrophobic interaction is ~ 100 times less than the particle diameter, and particle orientations can change by more than 10°. This justifies treating the angular interaction as sharply excluding certain orientations while not affecting the orientations of others, leading to the orientational entropy of Eq. (2). Similarly we may treat the hydrophobic central force interactions between bonded particles as harmonic in Eq. (9) owing to the smallness of the fluctuations. These approximations lead to a model which qualitatively describes the free energy of such a system, but quantitative tests of a particular experimental system would require incorporating more precise characterization of the hydrophobic interactions into a numerical calculation.

Simulations have examined both the kagome lattice in 2D[33] and the pyrochlore/HT lattices in 3D[22]. These simulations, which used a square-well attractive potential, found that the open lattices became stable when the bond strength was sev-

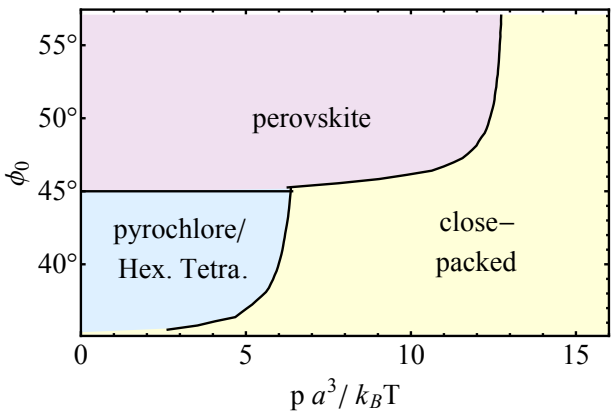

Fig. 10 Equilibrium phase diagram showing the transition between open and close-packed lattices. Open lattices are more able to fluctuate and are favored at high temperature, whereas high pressures favor the close-packed face-centered cubic lattice.

eral times temperature—strong enough for the lattice to condense from a fluid phase, but weak enough that bonds could break to escape from kinetic traps. In accordance with our own results, these simulations found that for a given patch size, the pressure at which the system transitioned from the close-packed to the open lattice was proportionate to the temperature. Our theory reveals the entropic mechanism of the stability of open lattices, and is able to capture the patch size dependence of the phase boundary.

4 Conclusion

In this paper, we discuss the self-assembly of three- dimensional open crystal lattices from patchy colloidal particles. We have shown that entropy of the particles not only stabilize these open lattices against mechanical instability, but also favor open structures over energetically equivalent close-packed ones.

The entropic mechanisms discussed in this paper provide a framework for designing simple building blocks for the self-assembly of colloidal open lattices. We show that by harnessing entropic effects, open lattices can spontaneously form without having to control surfacing pattern of colloidal particles beyond currently available experimental techniques: regular open lattices are favored by entropy.

5 Acknowledgments

We thank Qian Chen, Steve Granick, Tom Lubensky and Deshpreet Bedi for helpful conversations.

References

1 G. N. Greaves, A. L. Greer, R. S. Lakes and T. Rouxel, *Nat. Mater.*, 2011, **10**, 823–837.
2 K. Sun, A. Souslov, X. Mao and T. C. Lubensky, *Proc. Natl. Acad. Sci. U. S. A.*, 2012, **109**, 12369–12374.
3 J. N. Grima, R. Gatt, V. Zammit, J. J. Williams, K. E. Evans, A. Alderson and R. I. Walton, *J. Appl. Phys.*, 2007, **101**, –.
4 G. Ernst, C. Broholm, G. R. Kowach and A. P. Ramirez, *Nature*, 1998, **396**, 147–149.
5 K. D. Hammonds, M. T. Dove, A. P. Giddy, V. Heine and W. B., *Am. Mineral.*, 1996, **81**, 1057–1079.
6 C. L. Kane and T. C. Lubensky, *Nature Physics*, 2014, **10**, 39–45.
7 M. E. Davis and R. F. Lobo, *Chem. Mater.*, 1992, **4**, 756–768.
8 L. M. McDowellboyer, J. R. Hunt and N. Sitar, *Water Resour. Res.*, 1986, **22**, 1901–1921.
9 V. Kapko, M. Treacy, M. Thorpe and S. Guest, *Proc. R. Soc. London, Ser. A*, 2009, **465**, 3517.
10 A. Sartbaeva, S. A. Wells, M. M. J. Treacy and M. F. Thorpe, *Nat. Mater.*, 2006, **5**, 962–965.
11 D. W. Breck, *Zeolite molecular sieves: structure, chemistry, and use*, Wiley New York, 4th edn., 1973.
12 J. D. Joannopoulos, P. R. Villeneuve and S. H. Fan, *Nature*, 1997, **386**, 143–149.
13 A. Moroz, *Phys. Rev. B*, 2002, **66**, 115109.
14 A. J. Garcia-Adeva, *New J. Phys.*, 2006, **8**, 86.
15 J. F. Galisteo-Lopez, M. Ibisate, R. Sapienza, L. S. Froufe-Perez, A. Blanco and C. Lopez, *Adv. Mater.*, 2011, **23**, 30–69.
16 J. C. Maxwell, *Philos. Mag.*, 1864, **27**, 294.
17 H. Cohn and A. Kumar, *Proc. Natl. Acad. Sci. U.S.A.*, 2009, **106**, 9570–9575.
18 E. Edlund, O. Lindgren and M. N. Jacobi, *Phys. Rev. Lett.*, 2011, **107**, 085501.
19 S. Torquato, *Soft Matter*, 2009, **5**, 1157–1173.
20 K. P. Velikov, C. G. Christova, R. P. A. Dullens and A. van Blaaderen, *Science*, 2002, **296**, 106–109.
21 S. C. Glotzer and M. J. Solomon, *Nat. Mater.*, 2007, **6**, 557–562.
22 F. Romano and F. Sciortino, *Nat. Commun.*, 2012, **3**, 1–6.
23 A. V. Tkachenko, *Phys. Rev. Lett.*, 2002, **89**, 148303.
24 Q. Chen, S. Bae and S. Granick, *Nature*, 2011, **469**, 381–384.
25 S. Jiang, Q. Chen, M. Tripathy, E. Luijten, K. S. Schweizer and S. Granick, *Advanced Materials*, 2010, **22**, 1060–1071.
26 Q. Chen, E. Diesel, J. K. Whitmer, S. C. Bae, E. Luijten and S. Granick, *J. Am. Chem. Soc.*, 2011, **133**, 7725–7727.
27 X. Mao, Q. Chen and S. Granick, *Nature Materials*, 2013, **7**, 217.
28 X. Mao, *Phys. Rev. E*, 2013, **87**, 062319–33.
29 N. W. Ashcroft and N. D. Mermin, *Solid State Physics*, Saunders College, Philadelphia, 1st edn., 1976.
30 W. Setyawan and S. Curtarolo, *Computational Materials Science*, 2010, **49**, 299–312.
31 X. Mao and T. C. Lubensky, *Phys. Rev. E*, 2011, **83**, 011111.
32 L. V. Woodcock, *Nature*, 1997, **385**, 141–143.
33 F. Romano and F. Sciortino, *Soft Matter*, 2011, **7**, 5799–5804.